Contribution of numerical simulation for evaluation of the effect of section details and partial streamlining on the aerodynamic behaviour of bridge decks

L. Bruno *
Department of Structural Engineering, Politecnico di Torino, Torino, Italy.

S. Khris †
OptiFlow, Consulting Company in Numerical Fluid Mechanics, Marseille, France.

J. Marcillat ‡
Institut de Recherche sur les Phénomènes Hors Equilibre UMR 6594 UM-UP CNRS, Marseille, France.

Abstract

Presented herein is a numerical study for evaluating the aerodynamic behaviour of equipped bridge deck sections. In the first part, the method adopted is described, in particular concerning turbulence models, meshing requirements and numerical approach. The validation of the procedure represents the aim of the second part of the paper: the results of the numerical simulation in case of two-dimensional, steady, incompressible, turbulent flow around a realistic bridge deck are compared to the data collected from wind-tunnel tests. In order to demonstrate the influence of the section details and of the partial streamlining of the deck geometry on its aerodynamic behaviour, in the third part of the paper the effect of the fairings and of each item of equipment of the section (such as central barriers, side railings and sidewalks) is evaluated. The study has been applied to the deck section of the Normandy cable-stayed bridge.

1 Introduction

Wind-tunnel tests have traditionally been considered the most reliable method for investigating bluff body aerodynamics, even though they are relatively expensive and time-consuming. With the rapid increase in computer capacity and the recent developments in Computational Fluid Dynamics (CFD), numerical simulation of flows has become a cost-efficient and increasingly accurate approach.

*Assistant Professor
†Senior Analyst
‡Research Director

Careful research is called for to apply these numerical tools, which are already employed with considerable success in the aeronautics field, to wind engineering and in particular to bridge deck aerodynamics. Computation of flows around a bridge deck continues to present three main difficulties. Firstly, the Reynolds number related to such flows is very high ($Re \approx 1.e{+}07$). Such a large dimensionless number can rarely be satisfied in wind-tunnel tests. In numerical analysis, respecting this number involves particular requirements in spatial discretization, especially when grid-based methods are adopted. Secondly, the atmospheric boundary layer is highly turbulent. In experimental tests, boundary-layer wind tunnels ensure correct simulation of this flow characteristic. As regards CFD, turbulence models have to be adopted, and their effectiveness assessed. Thirdly, the actual finished bridge deck carries several items of equipment, such as side railings, crash barriers, sidewalks or side fairings. According to various authors, the effects of such section-model details cannot be disregarded. Using wind-tunnel tests, Bienkiewicz (1987) or Nagao et al. (1993) showed the influence of partial streamlining and traffic barriers on the vortex-induced response of bridge decks. Adopting the same approach, Scanlan et al. (1995) indicated the critical dependence of bridge flutter derivatives upon even minor details, such as deck railings. Furthermore, Scanlan considers the modelling of the section details as a critical component of wind-tunnel tests in terms of accuracy, as well as on account of the considerable investments both in time and in capital involved. Consequently, in any discussion of agreement with wind-tunnel test results, these items of equipment must be taken into account in numerical simulations, and the numerical approach must be validated in order to provide designers with a fully reliable tool of analysis.
Some authors, such as Selvam et al. (1999), Kuroda (1996) and Onyemelukwe et al. (1997) have recently applied computational methods to bridge aerodynamics. As regards grid-based methods, the current state of the art is mostly restricted to the simulation of smooth flows (i.e., without the use of turbulence models) around basic-shaped decks, that is, without considering the equipment. The purpose of the present paper is to tackle such difficulties by studying an actual case of turbulent flow around a full-detailed deck section.

2 Governing equations

2.1 *Turbulent-flow equations*

This study adopts the Reynolds averages of the governing partial differential equations of incompressible, viscous fluid flows. In the Reynolds averaging, the solution variables in the original Navier-Stokes equations are expressed as the sum of the mean and fluctuating components. Introducing such a decomposition of variables into the instantaneous continuity and momentum equations yields the Reynolds averaged Navier-Stokes (RANS) equations:

$$U_{i,i} = 0 \tag{1}$$

$$U_j U_{i,j} = -\frac{1}{\rho} P_{,i} + \left(\nu \left(U_{i,j} + U_{j,i}\right) - R_{ij}\right)_{,j} \tag{2}$$

where U_i is the mean velocity component in the i direction, P is the mean pressure, ρ is the specific mass, and ν is the molecular viscosity. The Reynolds stress $R_{ij} = \overline{u_i u_j}$ represents the effects of turbulence, which need to be modelled in order to close Equation 2.

2.2 *Reynolds stress expressions*

The turbulent constraints, which become apparent as a consequence of the non-linearity of the Navier-Stokes equations, are linked to the mean field by an isotropic turbulent viscosity ν_t. The Boussinesq assumption is based on analogy with the viscous-stress expression involved in laminar flows. The following linear model is established:

$$R_{ij} = \frac{2}{3}k\delta_{ij} - 2\nu_t S_{ij} \tag{3}$$

where $S_{ij} = \frac{1}{2}\left(U_{i,j} + U_{j,i}\right)$ is the mean field strain rate. The turbulent viscosity ν_t is expressed in terms of the turbulent kinetic energy k and its dissipation rate ε, as follows:

$$\nu_t = C_\mu \frac{k^2}{\varepsilon} \tag{4}$$

where the coefficient C_μ assumes different values according to the turbulence model adopted to express k and ε.

2.3 *$k - \varepsilon$ models*

In this paper, turbulence is computed using "two-equation" models based on the $k - \varepsilon$ model.
In the standard model, the turbulent kinetic energy k and its dissipation rate ε are established with regard to their transport according to the Jones & Launder (1972) model, as follows:

$$k_{,t} + U_j k_{,j} = -R_{ij}U_{i,j} + \left(\frac{\nu_t}{\sigma_k}k_{,i}\right)_{,i} - \varepsilon \tag{5}$$

$$\varepsilon_{,t} + U_j \varepsilon_{,j} = -C_{\varepsilon_1}\frac{\varepsilon}{k}R_{ij}U_{i,j} + \left(\frac{\nu_t}{\sigma_\varepsilon}\varepsilon_{,i}\right)_{,i} - C_{\varepsilon_2}\frac{\varepsilon^2}{k} \tag{6}$$

Equations 1, 2, 5 and 6 form the closed system in U_i, P, k, ε unknowns. The turbulent diffusion term is modelled by means of a gradient transport hypothesis for each of the two equations, whereas the viscous diffusion term, which regards both equations, is neglected because of the high Reynolds number assumption.
In line with the semi-empirical nature of the model, the derivation of the various model constants relies on experiments and numerical optimization procedure. In accordance with Jones & Launder (1972), the following values are assumed:

$$\begin{array}{llll} C_\mu = 0.09, & C_{\varepsilon_1} = 1.44, & C_{\varepsilon_2} = 1.92. \\ \sigma_k = 1.00, & \sigma_\varepsilon = 1.30. & \end{array}$$

A high-Reynolds-number model of this sort is suitable for application in bridge aerodynamics, especially in the case of fully streamlined decks and on account of its CPU time economy and stable solution. On the other hand, the standard $k - \varepsilon$ model is insensitive to high pressure gradients and strains, like the ones developing in flow around bluff sections or around a number of adjacent walls, such as those represented by bridge-deck equipment (Khris & Marcillat, 1997).
The RNG $k - \varepsilon$ form, as proposed by Yakhot et al. (1992), introduces an additional production contribution term $(-\pi)$ in the dissipation rate equation (Eqn. 6):

$$\pi = C_\mu \eta^3 \frac{(1 - \eta/\eta_0)}{1 + \beta\eta^3}\frac{\varepsilon^2}{k} = B\frac{\varepsilon^2}{k} \tag{7}$$

where $\eta = \frac{k}{\varepsilon}\sqrt{2S_{ij}S_{ij}}$ is the parameter which characterizes the mean field shear.
The coefficient C_{ε_1} (Eqn. 6) can be rewritten as follows:

$$C^*_{\varepsilon_1} = C^{\cdot}_{\varepsilon_1} - \eta\frac{(1-\eta/\eta_0)}{1+\beta\eta^3} \tag{8}$$

With the boundary-layer equilibrium assumption, where $\eta = \frac{1}{\sqrt{C_\mu}}$, a relation between the von Karman constant κ and the coefficient β can be deduced and written as follows: $\kappa = \left(\sigma_\varepsilon\left(C_{\varepsilon_1} - C^*_{\varepsilon_1}\right)\sqrt{C_\nu}\right)^{1/2}$.
The numerical coefficient values are determined analytically as follows:

$$\begin{array}{lll} C_\mu = 0.085, & C_{\varepsilon_1} = 1.42, & C_{\varepsilon_2} = 1.68 \\ \kappa = 0.387, & \eta_0 = 4.28, & \beta = 0.012, \\ \sigma_k = 0.718, & \sigma_\varepsilon = 0.718, & \end{array}$$

The above introduction of a rate-of-strain term in the transport equation for ε significantly improves the ability of this model to treat non-equilibrium effects in separated, recirculating, rapidly strained, time-dependent flows with large-scale organized structures (vortex shedding). For these reasons, its use is particularly suitable in simulating the flow around bluff, equipped bridge-deck sections. On the other hand, owing to this extra term, computations using the RNG model tend to occupy more CPU time than those using the standard model and tend to be more liable to instability (Fluent, 1996).

2.4 *Near-wall region*

The turbulence models described above are valid for turbulent core flows. In the case of wall-bounded flow, the regions close to walls are strongly affected by the presence of the wall. Firstly, the mean velocity field must satisfy the no-slip condition imposed at the wall boundary. Secondly, also turbulence is influenced: very close to the wall (viscous sublayer) the flow is almost laminar, and viscosity plays a dominant role in momentum transfer; in the outer sublayer of the near-wall region, turbulence is rapidly augmented due to high Reynolds stresses and to the large gradient of mean wind speed. For these reasons, near-wall modelling has a significant impact upon the reliability of the numerical solution. In this paper an attempt is made to arrive at a satisfactory near-wall modelling tool, using the wall-functions approach, where semi-empirical functions are imposed to solve the viscous sublayer and to ensure the profile continuity between the viscosity-affected region and the fully turbulent region.
In the Launder wall functions, the law-of-the-wall for mean velocity, in the formulation proposed by Launder & Spalding (1974), yields

$$U^* = \frac{1}{\kappa}\log Ey^* \qquad \text{if} \qquad y^* \geq 11.225 \tag{9}$$

$$U^* = y^* \qquad \text{if} \qquad y^* < 11.225 \tag{10}$$

where

$$U^* \equiv \frac{UC_\mu^{1/4}k^{1/2}}{\tau_w/\rho} \tag{11}$$

and the wall unit y^*

$$y^* \equiv \frac{C_\mu^{1/4}k^{1/2}y}{\nu} \tag{12}$$

The von Karman constant κ is equal to 0.42, and the empirical coefficient E assumes the value 9.81. The production of kinetic energy G_k and its dissipation rate ε at the wall-adjacent cells are computed on the basis of the assumption of a local equilibrium between production and dissipation source terms.

$$G_k \approx \tau_w \frac{\partial U}{\partial y} = \tau_w \frac{\tau_w}{\kappa \rho C_\mu^{1/4} k^{1/2} y} \tag{13}$$

$$\varepsilon = \frac{C_\mu^{3/4} k^{3/2}}{\kappa y} \tag{14}$$

The local equilibrium hypothesis restricts the applicational domain of such wall functions to a description of simple shear flow.
The so-called non-equilibrium wall functions are taken into account in order to overcome the limitations of the Launder functions and to ensure a reliable analysis for flows characterized by severe pressure gradients and strong non-equilibrium situations. Such a goal is achieved by means of two key elements. First, Launder's log law for the mean velocity is made sensitive to pressure gradient effects by adding an additional term to the velocity U in Equation 11

$$-\frac{1}{2}\frac{dp}{dx}\left[\frac{y_v}{\rho \kappa k^{1/2}} \log\left(\frac{y}{y_v}\right) + \frac{y - y_v}{\rho \kappa k^{1/2}} + \frac{y_v^2}{\nu \rho}\right] \tag{15}$$

where y_v is the physical viscous sublayer thickness, expressed by

$$y_v \equiv \frac{\nu y_v^*}{C_\mu^{1/4} k^{1/2} y} \tag{16}$$

Second, the near-wall cells are assumed to consist of a viscous and a fully turbulent sublayer. The cell-averaged production of k and of ε are then made sensitive to the thickness of the viscous sublayer, and the local equilibrium assumption is relaxed (Fluent, 1996).

2.5 *Boundary conditions*

The experimental tests used as references for the present study were not performed in boundary-layer wind tunnels. For this reason the inlet flow speed gradient is assumed as being equal to zero.
Provided that the variables are dimensionless with regard to the upstream flow velocity U_∞ and deck length B, the boundary conditions prescribed along the inlet section are of the Dirichlet type ones and are expressed as follows:

$$U = \cos\alpha, \quad V = \sin\alpha,$$
$$k = 1.5 I_t^2, \quad \varepsilon = \frac{k^{3/2}}{0.1\Delta},$$

where U and V are the non-dimensional horizontal and vertical velocities, I_t is the upstream turbulence intensity, α is the apparent angle of attack, and Δ is the turbulent characteristic length scale.
Free conditions are applied at the outlet boundary, as follows:

$$U_{,x} = 0, \quad V_{,x} = 0,$$
$$k_{,x} = 0, \quad \varepsilon_{,x} = 0,$$

Finally, adherence and equilibrium conditions are applied at the deck wall and at the first cell boundary for velocities and turbulent variables, respectively:

$$U = 0, \quad V = 0, \quad k_{,y_n} = 0, \quad \varepsilon = \left(C_\mu^{1/2} k_1\right)^{3/2} (\kappa y_n)^{-1}$$

where y_n is the normal to the wall ordinate and k_1 is the kinetic energy value at the first cell boundary.

3 Numerical approach

Computations were carried out using the FLUENT numerical code, based on the Finite Volume Method. Once the computational grid is generated, the differential conservation equations are converted to algebraic equations for discrete unknowns by means of integration about each control volume. Then the discretized segregated governing equation set is numerically solved by means of an iterative procedure. Bearing in mind the complex flow to be simulated in this study, the discretization scheme adopted is a first-order upwind one for both convection and viscous terms of each governing equation in order to avoid numerical diffusion. As regards choice of solvers and algorithm, the present study benefits from the work of Haroutunian et al. (1991) and Khris & Marcillat (1997) and adopts the consistent variant of the SIMPLE algorithm. The convergence criterion is extended at a residue value equal to $1.e-4$ in order to assure the steadyness of the drag coefficient.
In the grid-based method simulation of flow around complex geometries, mesh generation takes on fundamental importance. In this study the computational domains are generated by coupling unstructured and structured mesh types by means of substructuring of the total grid. The structured mesh is preferred in the neighbourhood of the wall on account of the regular, rectangular volumes that ensure a more consistent application of the wall functions. Moreover, such an approach enables easy modification of the grid so as to perform parametric studies on mesh sensitivity. The distance from the wall at the wall-adjacent cells, usually measured in the wall unit y^*, must be determined by considering the range over which the log law is valid. It is known that this condition is verified for $30 < y^* < 100$. The unstructured mesh was used because of its capacity to bridge the near-wall area characterized by the finest grid with the outer zone of the computational domain, where grid refinement can be relaxed.

4 Applications and results

The turbulence models adopted in this study are identified as follows:
STDB: standard $k-\varepsilon$ model associated with Launder's wall functions;
RNGB: RNG $k-\varepsilon$ model associated with Launder's wall functions;
RNGB-noeq.fct.: RNG $k-\varepsilon$ model associated non-equilibrium wall functions.
The study case considers a simulation of the flow around the Normandy cable-stayed bridge deck (Virlogeux, 1992). Table 1 summarizes the main characteristics of the flow configurations in various section model tests conducted for the wind design of the bridge. The adopted flow characteristics were

Table 1: Summary of flow characteristics.

Flow tests	Model scale	$U\ [m/s]$	I_t %	Re	$\alpha\ [deg]$
ONERA	1/75	32.3	0.1	$7.25e+5.$	$-6° \leq \alpha \leq +6°$
CEBTP	1/50	32.3	4	$1.05e+6.$	$-10° \leq \alpha \leq +10°$
CSTB	1/50	20.0	4	$6.5e+5.$	$-10° \leq \alpha \leq +10°$

the same as those established by ONERA in its wind-tunnel tests (Szechenyi, 1987). The data obtained by CEBTP and CSTB (Barre & Brebion, 1991 and Bietry & Grillaud, 1994) are also compared with the numerical results. In fact, even if such tests were characterized by slightly different flow configurations, Barre & Brebion (1991) demonstrated the insensitiveness of the aerodynamics coefficents

versus the Reynolds number in the range $1.64e+5. \leq Re \leq 6.56e+5$. The value of the turbulence characteristic length scale, which is not available in the literature, was set at $0.1B$ on the basis of a number of test cases. The deck section is characterized by a rather streamlined geometry due to the high slenderness of the box girder and to the further introduction of aerodynamic appendages at the edges. The deck is provided with side railings made up of three circular superimposed sections with a diameter of 0.005 in terms of non-dimensional deck chord length. The central railings have a square section with a dimension equal to $0.015B$; the averaged height of the sidewalk step is $0.011B$. Let us outline the small size of the details, which area represents less than 0.1% of the entire deck section area.

4.1 *Approach validation*

The effects of the position of the external boundaries, as well as the thickness of the first near-wall cell, were the subject of a preliminary study aimed at optimizing the spatial resolution. The domain and boundary conditions are depicted in Figure 1-a. The computational domain size is determined in

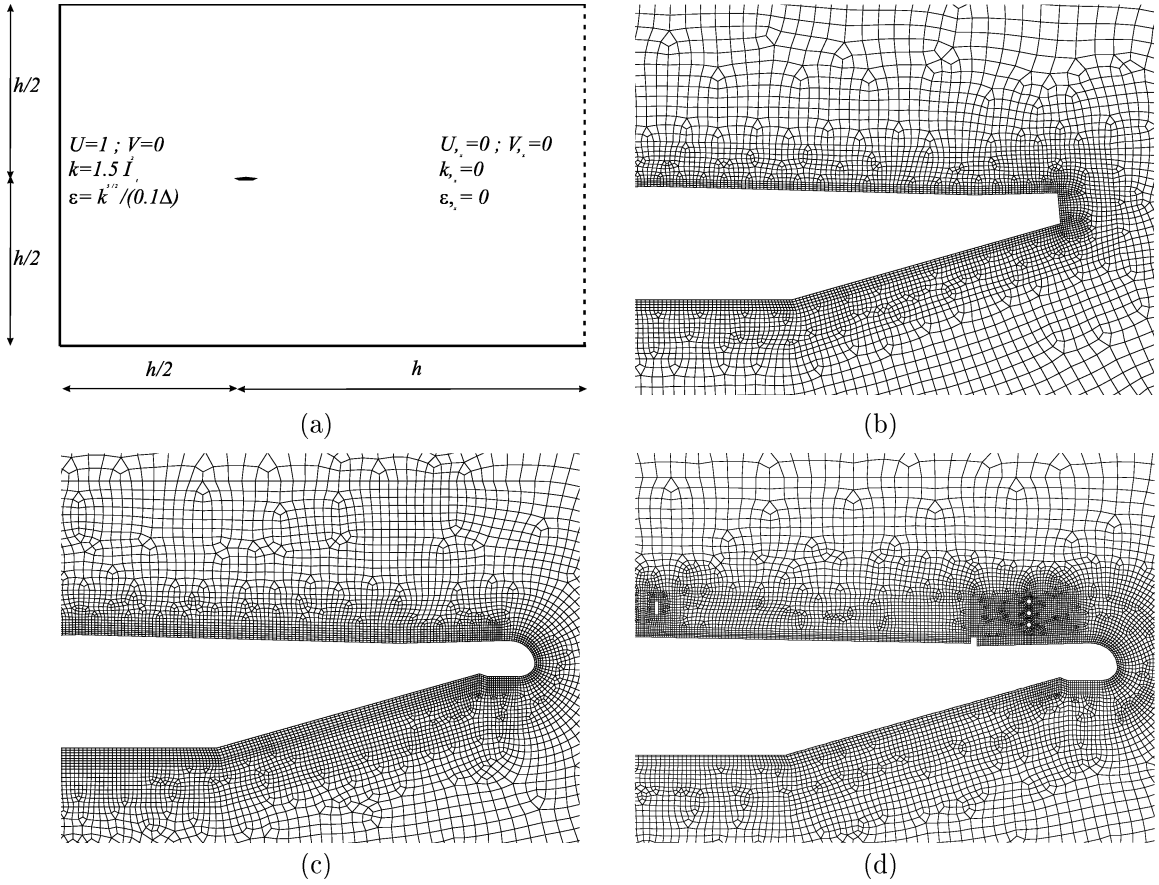

Figure 1: Computational domain and grid system near the investigated cross sections.

order to obtain solution insensitivity to the boundary condition and in order to limit the number of cells, i.e. to reduce the computational effort. Even if several domain sizes are tested in the present

study, in every model the ratio between its heigth h and width $w$is kept constant ($h = 2/3w$); the deck section is placed at a distance of one time the heigth upstream from the outlet boundary in order to enable proper simulation of the wake. Closed-up views of the optimized meshes generated around the structural deck section and around the streamlined and fully equipped sections are shown in Figure 1-b,c,d respectivelly.
In the fifth column of the table 2, the values of y^* obtained around the deck are shown: the significant values are those referred to a relatively undisturbed flow, such as the one on the underside of the deck. The grid "A", referred to the detailed geometry and characterized by a first cell thickness equal to $1.e-3$ in terms of deck chord length, yields values of y^* that are too low; i.e., it forces the log profile assumption in the viscous sublayer. An incremented value of the thickness ($y_{wc} = 2.e-3$) proves to be more suitable in conjunction with the assumed Reynolds number, resulting in correct values for the wall unit and a modification of the longitudinal velocity profile. Larger adjacent-wall cells are not to be envisaged if a correct simulation of the geometry of the side railings, whose characteristic dimension is of the same order of magnitude of the cell thickness ($\approx 2.e-3$), is to be ensured.
The remaining part of table 2 refers to the study concerning the optimization of the domain size. It may be appreciated that the computational domain size is related not only to the section geometry as may be expected, but also to the first near-wall thickness. The above results can be explained by a numerical diffusivity related to the number of control volumes between the section wall and the boundaries. The grid "detailed C" is retained for the full detailed configuration (see Figure 1-d).

Table 2: Influence of computational domain size and wall-adjacent cell thickness on the pressure coefficient at upper and lower boundaries (notations in figure).

model ID	grid points	y_{wc}	domain size	$\bar{y^*}$	$\Delta\bar{C}_p$	$\bar{C}_p$
detailed A	$3.3e+4$	$1.e-3$	$30B \times 20B$	≈ 5	0.0237	0.006
detailed B	$2.5e+4$	$2.e-3$	$30B \times 20B$	≈ 40	0.0237	0.287
detailed C	$2.9e+4$	$2.e-3$	$50B \times 40B$	≈ 40	0.0132	0.012
detailed D	$3.5e+4$	$2.e-3$	$70B \times 60B$	not converged		

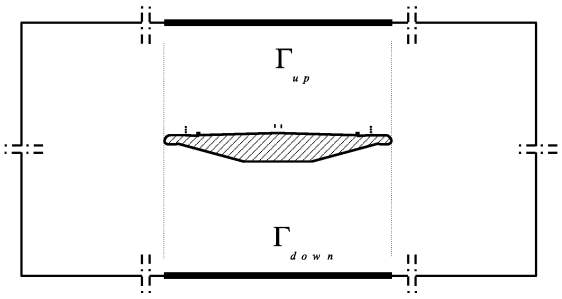

$$\bar{C}_{p_{up}} = \frac{1}{n_{\Gamma_{up}}} \sum_{i=1}^{n_{\Gamma_{up}}} C_{p_i}$$

$$\bar{C}_{p_{down}} = \frac{1}{n_{\Gamma_{down}}} \sum_{i=1}^{n_{\Gamma_{down}}} C_{p_i}$$

$$\Delta\bar{C}_p = \bar{C}_{p_{up}} - \bar{C}_{p_{down}}$$

$$\bar{C}_p = \frac{\bar{C}_{p_{up}} + \bar{C}_{p_{down}}}{2}$$

Pressure coefficient distributions on the deck found in wind-tunnel tests and in numerical simulations for an angle of attack equal to zero are compared in Figure 2. The insensitivity of the results to the turbulent models on the lower side of the deck is due to the simple shear flow caused by the extremely streamlined geometry. On the other hand, along the upper side the deck equipment involves non-equilibrium phenomena that depend upon the turbulence structure and its anisotropy, so that the choice of turbulence models and wall functions assumes greater importance. Generally speaking, the results are in overall good agreement around the entire section, except at the leading edge. The

prediction - which is common to all turbulence models - of a pressure deficit on the underside, due to an over-estimated velocity, is probably linked to the more marked blockage effect of the side railing and step on the upper side. It is our opinion that such discrepancies are mainly due to even just slight differences between the detail geometries reproduced in the wind-tunnel test and the ones modelled in the numerical simulation. The Cp distributions obtained using the RNG model provide a better fit

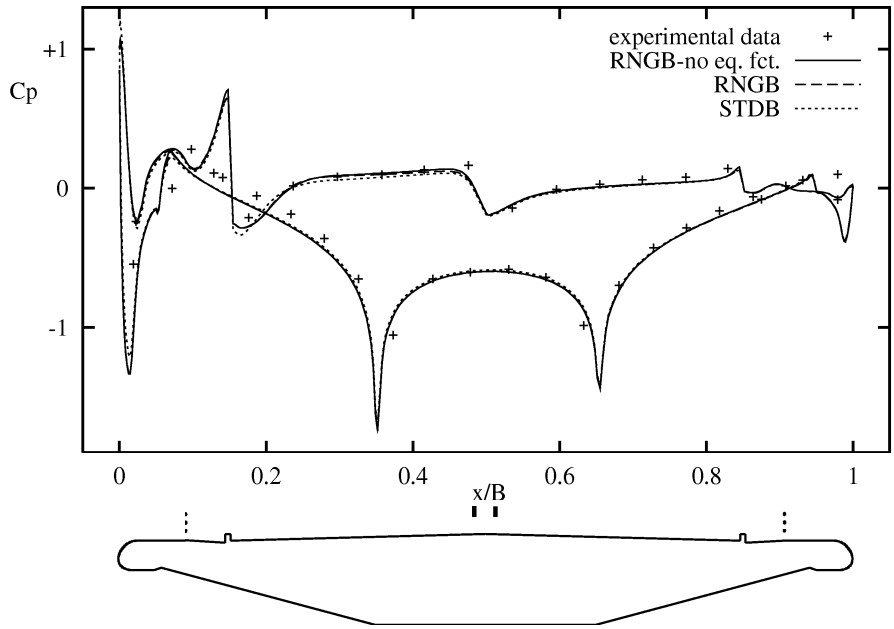

Figure 2: Pressure coefficient distribution on the deck.

with the experimental results for $0.15 < x/B < 0.65$; i.e., they yield a more satisfactory representation of the separated flow downstream of the leading-edge details.
Table 3 summarizes and compares the experimental and numerical results for the aerodynamic coefficients at an incidence equal to zero ($\alpha = 0°$). The discrepancy about the ONERA lift coefficient with respect to the value reported in Bruno *et all* 1999 is due to a previous error in reading the experimental data. The value of the lift coefficient was computed by ONERA by means of the integration

Table 3: Aerodynamic coefficients ($\alpha = 0°$ - definition of positive forces in figure).

Model	C_X	C_Y	C_M
STDB	+0.0693	−0.5151	−0.0151
RNGB	+0.0623	−0.5118	−0.0142
RNGB-noeq.fct.	+0.0626	−0.5294	−0.0148
ONERA	+0.0428	−0.357	+0.0139
CEBTP	+0.074	−0.452	+0.027
CSTB	+0.081	−0.388	+0.019

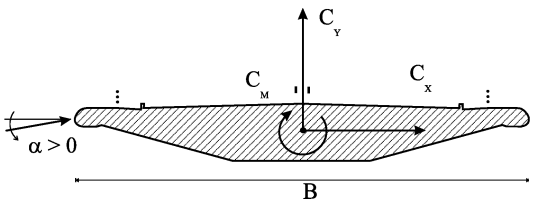

of pressure coefficient distribution; the drag coefficient value was obtained by the momentum theorem from measurements in the model wake; finally, the pitching moment coefficient was calculated at the elastic centre of the section. On the other hand, the experimental data proposed by CEBTP

(Barre & Brebion, 1991) and by CSTB (Bietry & Grillaud, 1994) refer to direct measurements of the aerodynamic forces. The aerodynamic coefficients values, numerically computed by integration of pressure and friction components, presents important differences with respect to the ONERA values ($\Delta C_X \approx 46\%$, $\Delta C_Y \approx 48\%$). With respect to the lift coefficient, such difference are strangely in contrast with the agreement recorded between the pressure coefficient distributions. Let us point out that, because of the small number of pressure taps, the experimental data neglect the local peaks of negative pressure at the lower surface of the deck. With respect to the drag coefficient, the recorded discrepancies are probably due to the insufficient precision of the numerical tools, but the occurrence of errors due to the experimental measuring apparatus cannot be excluded *a priori*. By the way, the experimental measurements obtained by CEBTP seem to confirm such hypothesis and support the quality of the numerical simulation.
Owing to the limited size of such details and the high Reynolds number, the recirculation zones involved are reduced in size and call for a close examination to be fully appreciated. The shear friction coefficient distribution for a limited range of x/B better highlights these phenomena, enabling the localization of the separation point (Fig. 3). The side railings involve a flow acceleration and then

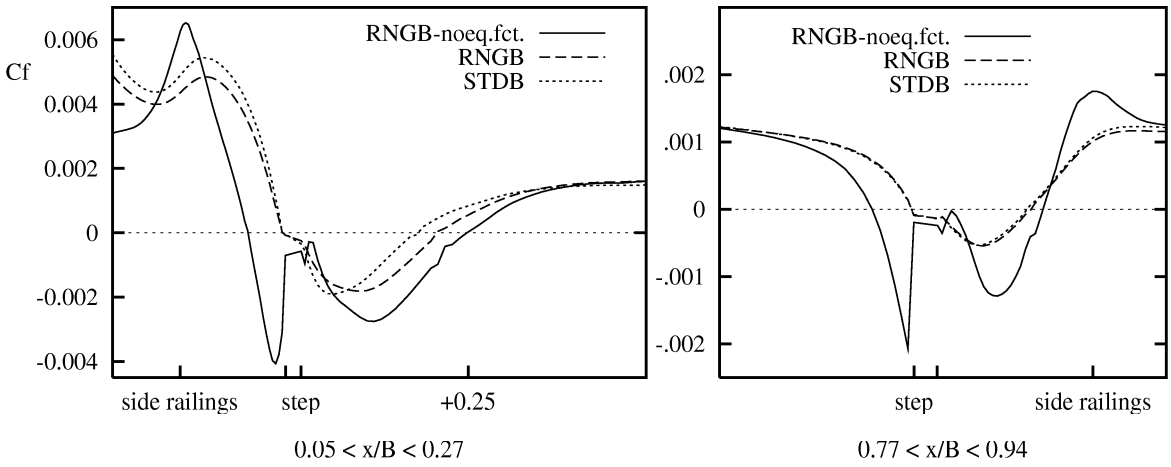

Figure 3: Shear friction coefficient distribution on the deck in neighbourhood of the side equipments.

a local peak in the Cf distribution located at the same abscissa ($x/B = 0.088$ and $x/B = 0.912$) when the RNGB-noeq.fct. model is used, whereas the other model combinations predict a delayed peak. The best benefits in the use of non-equilibrium wall functions result in the neighbourhood of the square-shaped step. Two recirculation regions appear upstream and downstream of the steps, in agreement with the kinematic investigations of Schofield & Logan (1990), while Launder's wall functions simulate only the second recirculation region. Furthermore, the downstream eddy size is underestimated by STDB because of its pure dissipative nature, whereas the RNGB sensitivity to the presence of rotation rate shifts the re-attachment point further downstream.

4.2 *Evaluation of the effect of equipment* - $\alpha = 0^{\circ}$

In this part of the paper the effect of each item of equipment (central and side barriers, steps, streamlined fairings) is evaluated by means of further simulations. Only the results of the best performing model - i.e. the RNGB-noeq.fct. - are reported for an angle of attack equal to zero. Firstly, the basic shaped section is modelled with streamlined fairings only. The changes in the geometry, and consequently in the nature of the flow, do not enable the same computational domain size as the one

adopted in the previous study to be kept, as follows from the mean Cp value at the inlet boundary given in Table 4. Result insensitivity is found for a domain size of $30B \times 20B$, with a substantial reduction in the number of nodes $n = 2.05e + 04$ (see Figure 1-c). The localized geometrical changes

Table 4: Influence of computational domain size and geometry on the pressure coefficient distribution at the upper and lower boundaries

model ID	domain size	y_{wc}	$\Delta\bar{C}_p$	$\bar{C}_p$
detailed C	$50B \times 40B$	$2.e-3$	0.013	$+0.01$
fairings A	$50B \times 40B$	$2.e-3$	0.005	-0.19
fairings B	$30B \times 20B$	$2.e-3$	0.006	$+0.003$

involved by the removal of the fairings do not involve significant modifications of the spatial discretization, characterized by a domain size of $30B \times 20B$ and a number of nodes equal to $n = 1.7e + 04$ (see Figure 1-b).
As pictured in Figure 4, the effect of details on the aerodynamic behaviour of the deck section is not just confined to their neighbourhood but also extends to the underside. The shear flow around the

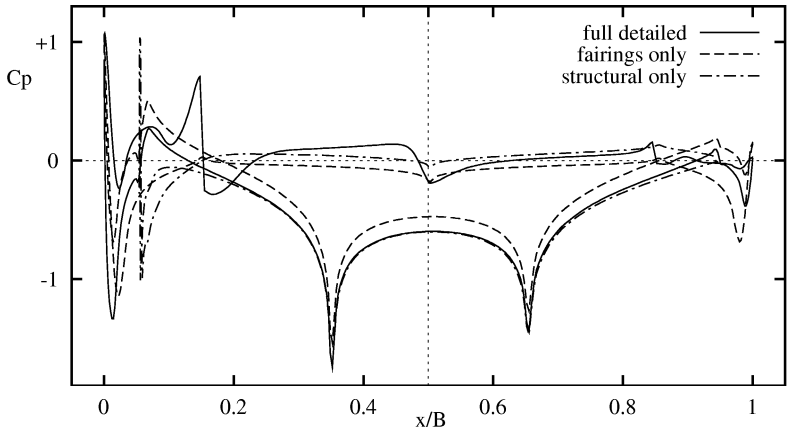

Figure 4: "Full-detailed", "fairings only" and "structural only" geometries: comparison between pressure coefficient distributions.

"fairings only" section is somewhat simpler if the large strains induced at the edges by the fairings are excluded. The absence of obstacles on the upper side of the deck involves a less pronounced velocity difference between the upper and lower zones. Then, a reduced scatter between the pressure level on the underside and on the upperside follows. Finally, the pressure coefficient presents a more symmetrical distribution in the "fairings only" section than in the other configurations with respect to the vertical axis passing through the elastic centre of the deck. It results from the pressure coefficient distribution referred to the structural section (no fairings) that the geometric configuration of the leading and trailing edges strongly affects the entire nature of the flow around the deck.
Consistently with the Cp distribution, the magnitude of the aerodynamic forces is directly related to the level of steamlining of the deck section (see Table 5). Generally speaking, a significant growth of the static wind effects on the deck follows, i.e. the neutral aerodynamic behaviour obtained in the design phases is vanished by the introduction of the equipment or by the removal of the appendages. In particular, the lift coefficient is dramatically increased in the "fairings only" configuration with

Table 5: Comparison between different levels of equipment: aerodynamic coefficients ($\alpha = 0$).

Model	C_X	C_Y	C_M
full-detailed	$+0.0626$	-0.5294	-0.0148
fairings only	$+0.0276$	-0.1395	$+0.0095$
structural only	$+0.0345$	-0.4498	$+0.0133$
side railings	$+0.0629$	-0.3907	-0.0006
central barriers	$+0.0487$	-0.2501	-0.0032
steps	$+0.0370$	-0.3656	$+0.0057$

respect to the "full detailed" one ($\Delta C_Y \approx 380\%$). Likewise, the pitching moment acting on the deck changes sign, so that the basic shaped section has a clockwise pitching behaviour. As may be expected, drag forces are markedly increased ($\Delta C_X \approx 126\%$) in the presence of details.
The unsymmetrical distribution of pressure involves an increased clockwise pitching moment acting on the structural deck, compared to the streamlined and full-detailed sections. As may be expected, the lift coefficient of the structural section is geatly decreased related to the streamlined one, nearly reaching the value obtained in the full detailed configuration.
The other rows of Table 5 regard the aerodynamic coefficients of the deck equipped with one detail at a time, in order to isolate the effect of each detail and to suggest possible qualitative design pointers. As may be appreciated, side railings have the biggest effect on aerodynamic forces, and particularly on drag. Pitching moment is much more sensitive as regards items of equipment located at a distance from the deck surface, i.e., side and central barriers, whereas sidewalk steps have no significant effects. The changes found in the lift component are significant for all obstacles located on the upper surface of the deck on account of the above-mentioned effect on the entire velocity field.
Figure 5 details information concerning the interaction between items of equipment by considering the local effects at the trailing edge on velocity profile and pressure coefficient distribution. In the full

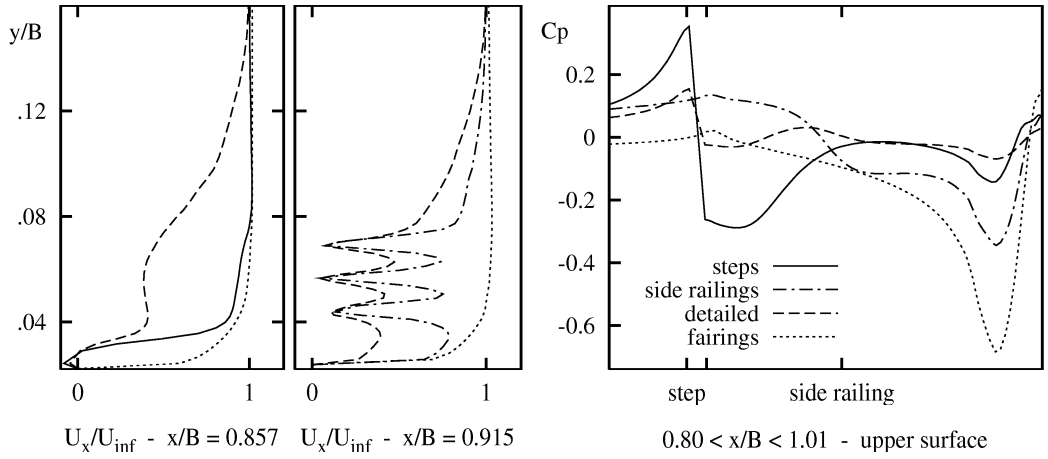

Figure 5: Local effect of steps and side railings on velocity profile and pressure coefficient distribution

detailed configuration, each detail is sheltered by the other items of equipment, so that incoming flow velocity is decreased, as also are the effects involved. Finally, as may be seen from Figure 6, equipment not only has a considerable influence on the deck but also considerably modifies the structure of the wake. A relevant modification of the wake structure and the raising of the local minimum in speed

profile are found especially as a result of the presence of side railings. As may be easily realized,

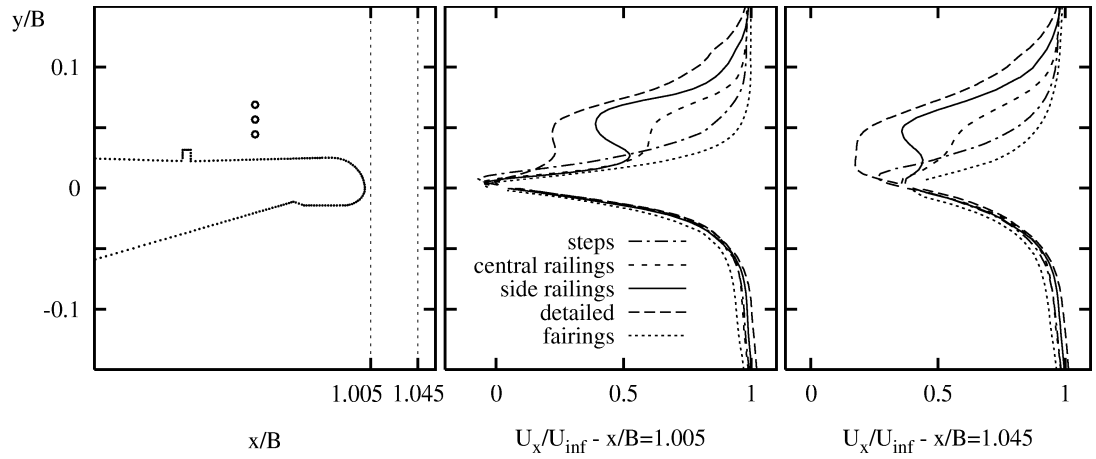

Figure 6: Streamwise velocity at two trailing wake locations for "fairings only", "full-detailed" and "single-detailed" geometries

the changes in the global behaviour of the deck involved by the removal of the streamlined fairings are due to local phenomena in proximity of the modified edges. In order to give details of the flow characteristics in proximity of the edges, let us comment on the closed-up views of streamlines at the leading and trailing tip (see Figure 7). At the leading edge of the structural configurations - see Figure 7 (f) - the flow is characterized by a boundary layer separation point localized at the bluff corner. The width of the recirculation zone in its downstream is easily appreciable by the skin friction coefficient plotted in (e) and directly related to walk side width in figure (d). On the other hand, the flow around the streamlined section is perfectly attached at the same edge. Finally, let us point out the different local incidence of the flow: in spite of the inlet flow has the same direction in both cases ($\alpha = 0$), the different slope of the leading point has a feedback influence on the flow. Then, the resulting local negative angle of attack to the structural deck well explains the decreased lift force observed in Table 6. At the trailing edge of the structural configurations - see Figure 7 (c) - the wake flow is characterized in proximity of the deck by two vortices, the upper one clockwise, the lower one counterclockwise. The velocity profile at two different locations in the wake confirms the recirculation zone in the neighborood of the deck. Morover, as previously described in Figure 6 with respect to the full detailed section, the increased velocity defect in the range $0.03 < y/B < 0.1$ confirms the increased dimensions of the wake.

4.3 *Evaluation of the effect of equipment* - $-6° \leq \alpha \leq +6°$

In this section, the study of the Normandy Bridge deck aerodynamics is extended to the range of incidences examined in the wind tunnel tests (see Table 1). The study is restricted to the three main configurations (i.e. the "full detailed", the "fairings only" and the "structural" ones). The evolution of the aerodynamic coefficients, defined in the profile axes (see Table 3), are plotted in figure 8. The table 6 summarizes the value of the aerodynamic coefficients and their derivatives with respect to the angle of attack ($dC_i/d\alpha\,(\alpha_0) = atan\,(\Delta C_i/\Delta\alpha)$ $[deg]$).

First at all, let us point out the large scatter between the experimental data, notably between the drag and lift coefficients recorded in ONERA and CSTB tests. The steady drag coefficient of the full detailed deck seems in good agreement with the mean values of the experimental data. On the other

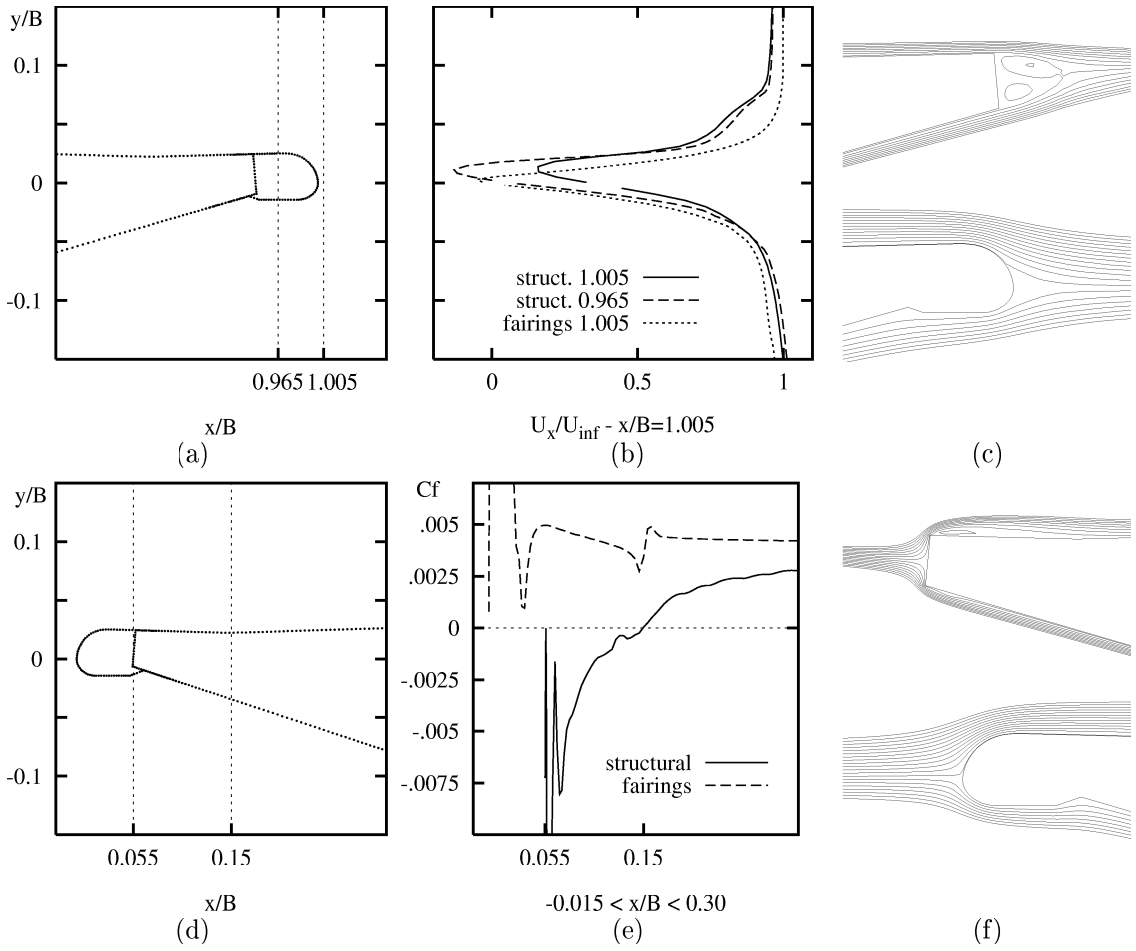

Figure 7: "Fairings only" and "structural only" geometries: comparison of relevant flow quantities in the neighborood of the trailing and leading edges.

hand the lift coefficient and its derivative are underpredicted in the range $-3 \leq \alpha \leq +6$. The same evolution can be observed for the pitching moment coefficient: in particular, the derivative remain approximativelly constant in the entire range of incidence, so that the numerical tool seems unable to predict the static instability of the deck due to torsional divergence (Virlogeux, 1992).

The safety equipments have a relevant effect on the aerodynamic behaviour, as emerges comparing the data related with the "full detailed" and "fairings only" configurations. In particular, the barriers modify both the C_X coefficient values and its derivatives, while they have no effects on the C_Y derivatives ($dC_Y/d\alpha\,(\alpha_0)_{detailed} = 3.23 \approx 3.62 = dC_Y/d\alpha\,(\alpha_0)_{fairings}$). It follows that such details do not dramatically affect the galloping stability in vertical flexion, according to the well known Den Hartog criterion ($dC_Y/d\alpha \geq 0$). On the other way, such data do not clarify in which way such details affect the bridge aerodynamic, i.e. in a direct or undirect way. In order to accomplish to this task, the direct contribution of details to the global drag and lift coefficients are plotted in Figure 9 and compared with the deck contribution in presence of the details ("full detailed") and without them ("fairings"). Two main remarks follow. Firstly, the direct contribution of the details to the drag coefficient is of

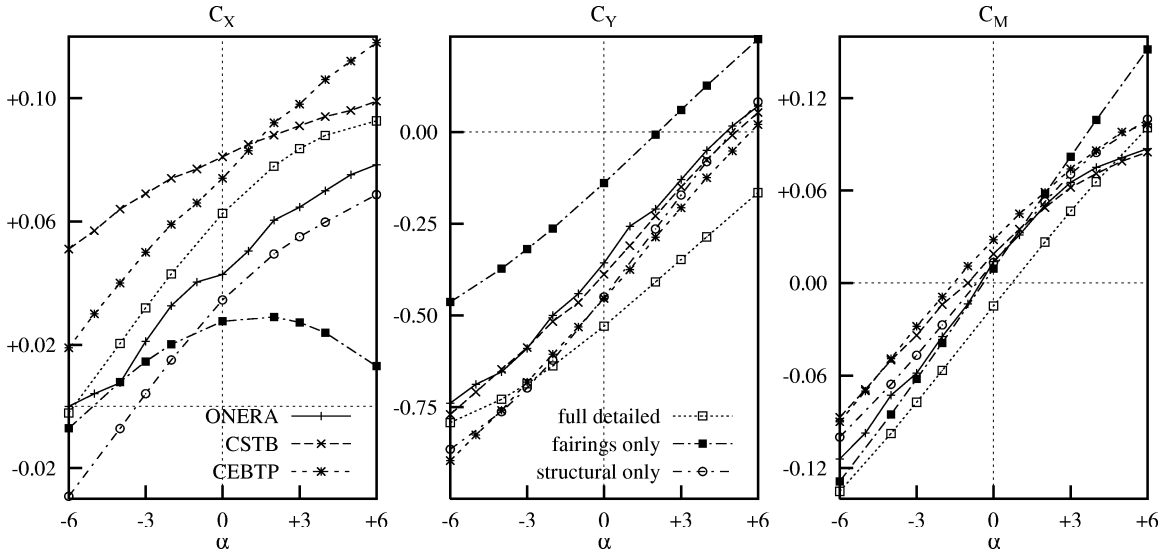

Figure 8: Comparison of the aerodinamic coefficients plotted versus the angle of attack.

Table 6: Aerodynamic coefficients ($\alpha = 0$) and their derivatives.

Model	C_X	C_Y	C_M	$dC_X/d\alpha\,(\alpha_0)$		$dC_Y/d\alpha\,(\alpha_0)$		$dC_M/d\alpha\,(\alpha_0)$	
				$\pm3°$	$\pm6°$	$\pm3°$	$\pm6°$	$\pm3°$	$\pm6°$
full-detailed	+0.0626	−0.5294	−0.0148	0.49	0.45	3.23	2.99	1.18	0.65
fairings only	+0.0276	−0.1395	+0.0095	0.12	0.10	3.62	3.42	1.38	1.34
structural only	+0.0345	−0.4498	+0.0133	0.49	0.47	5.01	4.51	1.12	0.98
ONERA	+0.0428	−0.357	+0.0139	0.42	0.37	4.38	3.86	1.18	0.96
CEBTP	+0.074	−0.452	+0.027	0.47	0.47	4.58	4.40	0.97	0.93
CSTB	+0.081	−0.388	+0.019	0.21	0.23	4.18	3.93	0.92	0.82

the same order of magnitude of the one related to the deck, but it remains approximativelly constant with respect to the incidence. So, the relevant difference in the C_X slopes obtained in the "fairings" and "full detailed" configurations follows from the deck component. This data confirms the radical change of the entire nature of the flow around the deck and in particular the relevant effects of the details in the wake (see Figure 6). Secondly, the direct contribution of the details to the lift coefficient is very small and remains constant in the examined range of incidence. Then, the undirect effects on the lift force acting on the deck are predominant with respect to the force intensity and its evolution versus the angle of attack. Such data, analized as an whole, demonstate the high level of aerodynamic interference between the deck and the equipments.

The stedy coefficients of the structural configuration unexpectedly fit with the experimental data better than the ones obtained from the "full detailed" configuration. The lift and the moment coefficients values and their derivatives are expecially in good agreement. Even if a definitive conclusion is not possible, in the opinion of the authors such result can be explained by the unachieved aerodynamic similarity of the safety barriers. Because of the very small size of such details, their porosity could be understimated in the model so to increase the "degree of bluffness" of the deck. In such a way, the side railings are analogous with a non-porous panel and the complete model is characterized by the

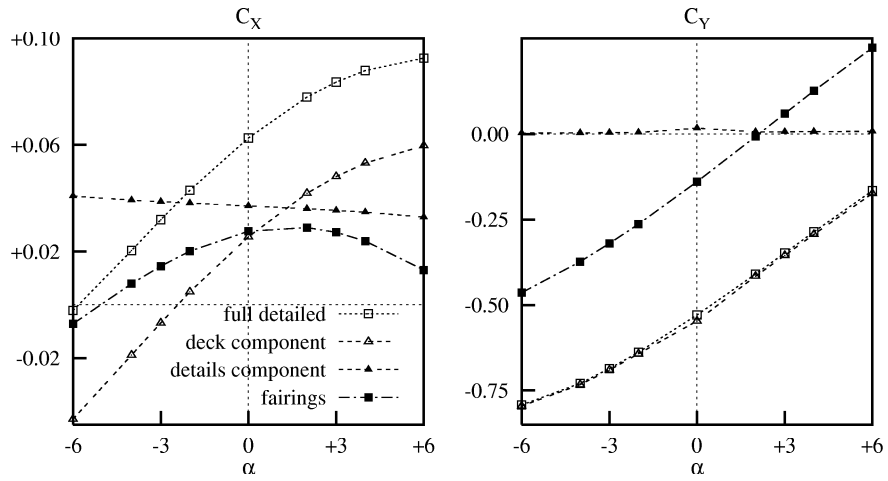

Figure 9: Direct and undirect effects of the section details on the aerodynamic forces.

same behaviour of the bluff structural section. The small scale of the model and the relatively low Reynolds number adopted in the experimental tests (see Table 1) seem to support such hipotesis.

5 Conclusions

The study based on the method adopted confirms the current suitability of CFD tools for predicting the flow around full-detailed bridge deck sections. As regards the tested turbulence models, the standard $k-\varepsilon$ model associated with standard wall functions is unable to reproduce the separation that often occur in flow around bluff bodies. Instead, the RNG model coupled with non-equilibrium wall functions emphasizes secondary eddy presence and correctly simulates the interaction between boundary layers and shear layers where a number of adjacent boundaries is present. The flexibility of the numerical approach makes it possible to exploit many and less expensive tests aimed to assessing various geometrical parameters in order to be complementary with wind-tunnel tests. As regards the effect of details on the aerodynamic behaviour of bridge decks, even minor changes made to the cross-sectional geometry by equipments or fairings have an important influence not only in the neighbourhood of their location, but also on the aerodynamic behaviour of the section as a whole. In particular, the trailing wake modifications and the separated flow at the leading edge suggest a possible influence of such details on the unsteady solution. For the above mentioned reasons, the study of the effect of details on deck response to vortex-shedding will be the subject of further investigations.

Acknowledgements

The Authors gratefully acknowledge Mr. Szechenyi and Mr. Grillaud for the kind availability of the experimental data.

References

Barre, C. and Brebion H. (1991), *"Coefficients Aerodynamiques Stationnaires du Tablier du Pont de Normandie Equipé de Corniches Arrondies"*,EN-AS 92.4 C, CSTB, Nantes.

Bienkiewicz, B. (1987), "Wind tunnel study of geometry modification on aerodynamics of a cable-stayed bridge deck",*J. Wind Eng. Ind. Aerod.*, 26(3) 325-339.

Bietry, J. and Grillaud, G. (1994), "Wind studies for the Normandy bridge", *Proceedings International Conference on Cable Stayed and Suspension Bridges*, Deauville, October.

Bruno, L., Khris, S., Marcillat, J. (1999), "Contribution of numerical simulation for evaluation of the effect of section details on the aerodynamic behaviour of a long span bridge deck", *Proceedings 10th International Conference on Wind Engineering*, Copenaghen, June.

Fluent (1996), *"Theory Manual"*, Lebanon: Fluent Incorporated.

Haroutunian, V. and Engelman, M. (1991), "On modelling wall-bound turbulent flows using specialized near wall finite elements and the standard $k-\varepsilon$ turbulence model", *Proceedings Symposium on Advances in Numerical Calculation of Turbulent Flows*, Portland, June.

Jones A.C. and Launder D.B. (1972), *"Lectures in mathematical models of turbulence"*, Academic Press, London.

Khris, S. and Marcillat, J. (1997), "Effects of first-order turbulence models applied to flows around lifting airfoils", *Proceedings of 11 Symposium on Turbulent Shear Flow*, Grenoble, September.

Kuroda, S. (1996), "Numerical simulation of flow around bridge", *Ihi Engineering Review*, 29(2), 59-66.

Launder, B.E. and Spalding D.B. (1974), "The numerical computation of turbulent flows", *Computer Methods in Applied Mechanics and Engineering*, 3 269-289.

Nagao, F., Utsunomiya, H., Oryu, T., Manabe, S. (1993) "Aerodynamic efficiency of triangular fairing on box girder bridge ", *J. Wind Eng. Ind. Aerod.*, 49, 565-574.

Onyemelukwe, O.U., Torkamani, M.A.M. and Bosch,H.R. (1997), "Numerical simulation of wind induced forces on bridge deck sections of long-span bridges",*Computer and Structures*, 62(4), 667-679.

Panneer Selvam, R. and Bosch, H.R. (1999), "Finite element modelling of flow around bridges", *Proceedings 10th International Conference on Wind Engineering*, Copenaghen, June.

Scanlan, R.H., Jones, N.P., Sarkar, P.P. and Singh, L. (1995), "The effect of section model details on aeroelastic parameters", *J. Wind Eng. Ind. Aerod.*, 54/55: 45-53.

Schofield, W.H. and Logan, E.(1990) "Turbulent shear flows over surface mounted obstacles", *Trans. of the A.S.M.E.*, vol 112: 376-385.

Szechenyi, E. (1987), *"Pont de Normandie: effets du vent; étude aéroélastique-essais"*, 10/3588 RY070R370G, ONERA, Paris.

Virlogeux, M. (1992), "Wind design and analysis for the Normandy bridge", *Proceedings First International Symposium on Aerodynamics of Large Bridges*, Copenaghen, February.

Yakhot, V., Orszag, S.A., Thangam, S., Gatski, T.B. and Speziale, G.C. (1992), "Development of turbulence models for shear flows by a double expansion technique", *Phys. Fluids*, A 4(7), 1510-1520.

key words

Computational Fluid Dynamic - Bridge Aerodynamics - Section model details.